Analysis of Solvent Nucleophile Isotope Effects: Evidence for Concerted Mechanisms and Nucleophilic Activation by Metal Coordination in Nonenzymatic and Ribozyme-Catalyzed Phosphodiester Hydrolysis†

Adam G. Cassano,‡ Vernon E. Anderson,*,§ and Michael E. Harris*,‡,§

Center for RNA Molecular Biology and Department of Biochemistry, Case Western Reserve University School of Medicine, Cleveland, Ohio 44106

Received April 22, 2004; Revised Manuscript Received May 28, 2004

ABSTRACT: Heavy atom isotope effects are a valuable tool for probing chemical and enzymatic reaction mechanisms; yet, they are not widely applied to examine mechanisms of nucleophilic activation. We developed approaches for analyzing solvent ^{18}O nucleophile isotope effects ($^{18}k_{nuc}$) that allow, for the first time, their application to hydrolysis reactions of nucleotides and nucleic acids. Here, we report $^{18}k_{nuc}$ for phosphodiester hydrolysis catalyzed by Mg^{2+} and by the Mg^{2+}-dependent RNase P ribozyme and deamination by the Zn^{2+}-dependent protein enzyme adenosine deaminase (ADA). Because ADA incorporates a single solvent molecule into the product inosine, this reaction can be used to monitor solvent $^{18}O/^{16}O$ ratios in complex reaction mixtures. This approach, combined with new methods for analysis of isotope ratios of nucleotide phosphates by whole molecule mass spectrometry, permitted determination of $^{18}k_{nuc}$ for hydrolysis of thymidine 5′-*p*-nitrophenyl phosphate and RNA cleavage by the RNase P ribozyme. For ADA, an inverse $^{18}k_{nuc}$ of 0.986 ± 0.001 is observed, reflecting coordination of the nucleophile by an active site Zn^{2+} ion and a stepwise mechanism. In contrast, the observed $^{18}k_{nuc}$ for phosphodiester reactions were normal: 1.027 ± 0.013 and 1.030 ± 0.012 for the Mg^{2+}- and ribozyme-catalyzed reactions, respectively. Such normal effects indicate that nucleophilic attack occurs in the rate-limiting step for these reactions, consistent with concerted mechanisms. However, these magnitudes are significantly less than the $^{18}k_{nuc}$ observed for nucleophilic attack by hydroxide (1.068 ± 0.007), indicating a "stiffer" bonding environment for the nucleophile in the transition state. Kinetic analysis of the Mg^{2+}-catalyzed reaction indicates that a Mg^{2+}−hydroxide complex is the catalytic species; thus, the lower $^{18}k_{nuc}$, in large part, reflects direct metal ion coordination of the nucleophilic oxygen. A similar value for the RNase P ribozyme catalyzed reaction provides support for nucleophilic activation by metal ion catalysis.

Phosphodiester hydrolysis is strongly favored thermodynamically but extremely slow kinetically (*1*), and so it is well suited for regulation by protein and RNA enzymes, which can catalyze the reaction $10^{12}-10^{14}$ fold (*2, 3*). Knowledge of the chemical mechanism for phosphodiester hydrolysis is intrinsic to understanding how this catalysis is achieved. Studies of model compounds show that phosphodiester cleavage can proceed by either a concerted mechanism involving simultaneous breaking of the leaving group bond and formation of the bond to the nucleophile (*4*−*6*) or a stepwise mechanism with formation of a phosphorane intermediate (*7*−*9*). Although both types of mechanism appear to be used by phosphodiesterase enzymes (*6*, *10*−*12*), the factors influencing which mechanism occurs are not fully understood.

Catalysis of either mechanism requires activation of the nucleophile and stabilization of the developing negative charge on the leaving group. Structural studies of phosphodiesterases show that such catalytic interactions are mediated in large part by divalent metal ion cofactors (*13*−*15*); however, there remains significant ambiguity concerning the precise number and roles of active site metal ions in the transition state. Large catalytic RNAs are also believed to employ active site metal ions for catalysis. However, in contrast to protein enzymes, information regarding active site metal ion interactions in ribozymes comes largely from "metal ion specificity switch" experiments, which indicate direct interactions between metal ions and the scissile phosphate in the group I (*16*, *17*) and group II introns (*18*) and ribonuclease P (RNase P)[1] (*19*, *20*) ribozymes. Such biochemical analysis has been applied to protein systems as

† Supported by NIH Grant GM56740 (M.E.H.) and a HHMI predoctoral fellowship (A.G.C.).

* To whom correspondence should be addressed. M.E.H.: e-mail, meh2@cwru.edu; phone, 216-368-4779; fax, 216-368-2110. V.E.A.: e-mail, vea@cwru.edu; phone, 216-368-2559.

‡ Center for RNA Molecular Biology, Case Western Reserve University School of Medicine.

§ Department of Biochemistry, Case Western Reserve University School of Medicine.

[1] Abbreviations: HAIE, heavy atom isotope effects; ADA, adenosine deaminase; RNase P, ribonuclease P; KIE, kinetic isotope effect; EIE, equilibrium isotope effect; T5PNP, thymidine 5′-*p*-nitrophenyl phosphate; TMP, thymidine monophosphate; 3ClQ, 3-chloroquinuclidine; ESI-QMS, electrospray ionization quadrupole mass spectrometry; SIM, single ion monitoring; IRMS, isotope ratio mass spectrometry; pGp, guanosine 3′,5′-bisphosphate; TIF, temperature-independent factor; TDF, temperature-dependent factor.

10.1021/bi049188f CCC: $27.50
Published on Web 07/22/2004

well (*21*). Unfortunately, this strategy is not practical for examining interactions with a solvent nucleophile. As a result, it remains difficult to directly test models of enzyme-catalyzed phosphodiester hydrolysis that invoke activation of a solvent nucleophile by metal ion coordination.

Heavy atom isotope effects (HAIE) are a useful tool for probing chemical and enzymatic mechanisms (*22*−*24*). Analysis of HAIE provides information regarding differences in the "stiffness" of the bonding environment of the isotopically substituted atom between either the reactants and the products [from equilibrium isotope effects (EIE)] or the reactants and the transition state [from kinetic isotope effects (KIE)] (*25*). This property makes HAIE useful for determining whether bond formation to the nucleophile occurs before, during, or after the rate-limiting transition state of phosphodiester hydrolysis reactions and, therefore, for differentiating between concerted and stepwise mechanisms. Because they are present in the transition state structure, KIEs also detect changes in bond stiffness due to equilibria upstream of the chemical step, such as metal coordination or deprotonation.

HAIE of phosphate oxygens have been used to examine the mechanism of nonenzymatic phosphodiester hydrolysis, providing a useful framework for interpreting effects from enzymes (*6*, *9*, *26*, *27*). For diesters with good leaving groups, normal isotope effects on both the leaving group and nucleophile are observed, indicative of a concerted mechanism. Nonbridging oxygen effects are small and inverse, characteristic of a slightly dissociative transition state. These data have been interpreted as showing that hydrolysis of phosphodiesters with reactive leaving groups occurs by concerted mechanisms with early transition states. An important exception is catalysis by a dinuclear Co^{3+} complex in which a large inverse nucleophile isotope effect is observed, consistent with a stepwise mechanism involving equilibrium formation of an intermediate in which the new bond to the nucleophile is fully formed (*9*). Protonation of the nucleophile or the phosphate oxygens can influence the degree of stiffness in the transition state bonding environment, and equilibrium deprotonation to yield hydroxide results in a large normal contribution to the observed nucleophile isotope effect for alkaline hydrolysis of a model diester of *p*-nitrophenol (*27*). Additionally, inverse nonbridging oxygen isotope effects provide evidence for protonation of these positions during acid-catalyzed hydrolysis and for cleavage catalyzed by phosphodiesterase I (*6*).

While HAIE have been used extensively for mechanistic studies of protein enzymes (*10*, *23*, *28*, *29*), their application to catalytic RNAs has been limited (*30*). This situation is not due to lack of interest but to the combined technical challenges of isolating the scissile phosphate from macromolecular products and measuring small changes in $^{18}O/^{16}O$ or $^{33}P/^{31}P$ isotope ratios with the requisite precision. Despite these difficulties, the mechanistic information from such analyses would help to extend our understanding of ribozyme mechanisms and contribute to comparisons of the relative capabilities of RNA and protein active sites (*31*).

One ribozyme where analysis of nucleophile HAIE would be particularly useful for probing mechanism is ribonuclease P (RNase P), which is unique among naturally occurring ribozymes because its biological function is to catalyze phosphodiester hydrolyses. RNase P requires divalent metal

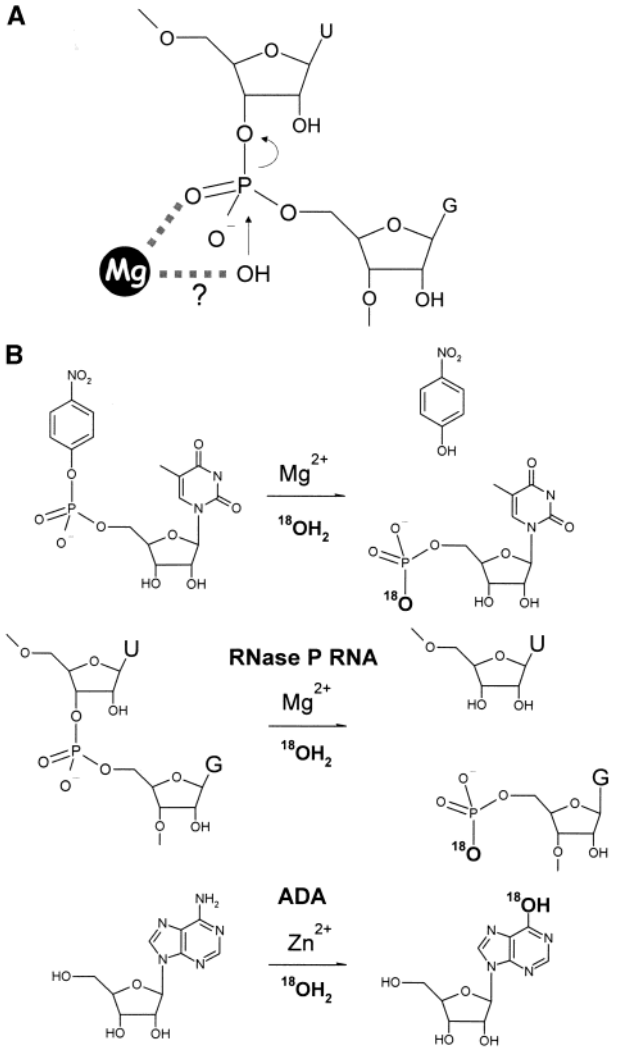

FIGURE 1: (A) Metal ion catalysis by nucleophilic activation in enzymatic phosphodiester hydrolysis. Active site divalent metal ions, most commonly Mg^{2+}, interact simultaneously via direct inner-sphere coordination with a nonbridging oxygen and the nucleophilic water molecule. Metal ion coordination is proposed to promote catalysis by lowering the pK_a of the bound water to increase the concentration of hydroxide, which acts as the nucleophile. Additionally, simultaneous interaction between the phosphate and hydroxide can assist in positioning the nucleophile for in-line attack. (B) Incorporation of solvent nucleophile into nucleotide phosphates by Mg^{2+}-, ribozyme-, and ADA-catalyzed hydrolyses.

ions for activity, and extensive kinetic and structure−function evidence strongly suggests that at least one active site metal ion participates directly in catalysis (*19*, *20*, *32*, *33*). Current models for the RNase P catalytic mechanism (Figure 1) propose nucleophilic activation by metal ion coordination (*34*, *35*), but as with the majority of analogous protein phosphodiesterases, no direct test of this hypothesis has been made.

To better understand mechanisms of nucleophilic activation in enzymatic and nonenzymatic phosphodiester hydrolysis reactions, we developed approaches for isolation and analysis of nucleotides containing the reacted phosphate and determination of the isotopic composition using whole molecule mass spectrometry. Using these approaches we measured the ^{18}O isotope effect on the water nucleophile ($^{18}k_{nuc}$) for the reaction catalyzed by the RNase P ribozyme and for a model aqueous reaction catalyzed by Mg^{2+} (Figure

1B). For the RNase P reactions, we determined the solvent $^{18}O/^{16}O$ ratio by monitoring incorporation of solvent into the inosine product of the hydrolytic deamination of adenosine catalyzed by adenosine deaminase (ADA). This technique required the determination of $^{18}k_{nuc}$ for the ADA reaction. The observed inverse isotope effect for ADA reflects a large increase in bond stiffness due to coordination of the nucleophile by an active site Zn^{2+} ion and a stepwise mechanism involving formation of a tetrahedral intermediate. In contrast, $^{18}k_{nuc}$ for the Mg^{2+}-catalyzed phosphodiester hydrolysis reaction is normal, yet significantly lower in magnitude than $^{18}k_{nuc}$ for the hydroxide-catalyzed reaction (*27*). These results are consistent with a concerted reaction mechanism with an increased stiffness in the bonding environment of the nucleophile resulting from coordination to a catalytic metal ion, and this model is further supported by kinetic analysis. The intrinsic isotope effect for the RNase P catalyzed reaction is also normal and similar in magnitude to the Mg^{2+}-catalyzed model reaction. These results confirm models of RNase P catalysis invoking a concerted mechanism and provide evidence consistent with nucleophilic activation by metal ion coordination.

MATERIALS AND METHODS

Determination of Solvent Nucleophile Isotope Effects. $^{18}k_{nuc}$ KIEs for water as the nucleophile have been determined previously by three different procedures: direct comparison (*36*), equilibrium perturbation (*37*), and isotope ratio determinations (*29*). Direct comparison studies are prone to the errors associated with running parallel reactions, and equilibrium perturbation is not applicable to the essentially irreversible phosphodiester hydrolysis. The use of isotope ratio measurements to study $^{18}k_{nuc}$ for hydrolysis reactions was first applied to carboxypeptidase (*29*). The irreversible hydrolysis of a phosphodiester is shown in eq 1

$$H_2{}^{18}O/H_2{}^{16}O + \text{phosphodiester} \rightarrow ROP(^{18}O)O_2{}^{2-} + ROP(^{16}O)O_2{}^{2-} + HOR'$$

$$^{18}k_{nuc} = (H_2{}^{18}O/H_2{}^{16}O)/\{[ROP(^{18}O)O_2{}^{2-}]/[ROP(^{16}O)O_2{}^{2-}]\} \quad (1)$$

and diagramed in Figure 1B with the isotopic composition of the water and of the product phosphate ester explicitly noted. Because the solvent is present in vast excess, its isotope ratio is not altered by the reaction. Consequently, the isotope ratio of the product is also unchanged during the reaction. In this case the $^{18}k_{nuc}$ is determined by measuring the isotope ratio of both the water and the product monophosphate ester.

Since neither isotope ratio varies as a fraction of reaction, the reaction can be run arbitrarily near to completion. However, unlike the standard competitive measurements, the isotope ratio of two different molecules must be determined. This introduces the potential for systematic error if the two methods of isotope ratio analysis have different instrumental biases. Two different novel methods are described that limit this potential source of error in the determination of $^{18}k_{nuc}$ for hydrolysis reactions.

The first method was applied to the ADA reaction shown in eq 2. Aside from the oxygen incorporated at the 6 position

$$H_2{}^{18}O/H_2{}^{16}O + \text{adenosine} \rightarrow (6\text{-}^{18}O)\text{inosine} + (6\text{-}^{16}O)\text{inosine} \rightarrow (6\text{-}^{18}O)\text{hypoxanthine} + (6\text{-}^{16}O)\text{hypoxanthine}$$

$$^{18}k_{nuc} = (H_2{}^{18}O/H_2{}^{16}O)/\{(6\text{-}^{18}O)\text{inosine}/(6\text{-}^{16}O)\text{inosine}\} \quad (2a)$$

$$^{18}k_{nuc} = (H_2{}^{18}O/H_2{}^{16}O)/\{(6\text{-}^{18}O)\text{hypoxanthine}/(6\text{-}^{16}O)\text{hypoxanthine}\} \quad (2b)$$

of the purine base, all of the other oxygens in inosine are contributed by the ribose moiety; thus, purification of the nucleobase hypoxanthine permits efficient isolation of the incorporated oxygen isotope (Figure 1B).

Recent developments in continuous-flow isotope ratio mass spectrometry make it possible to convert both water and hypoxanthine to C≡O by anoxic thermal decomposition in a glassy carbon reactor. The $C{\equiv}^{18}O/C{\equiv}^{16}O$ isotope ratio can then be determined on-line with an isotope ratio mass spectrometer at natural abundance (*38*, *39*). Thus, for the ADA reaction, the water and the product isotope ratios using only natural abundance ^{18}O are determined in the same analyte (C≡O) with the same instrument, minimizing the instrumental bias. If the conversion of water or hypoxanthine to C≡O is incomplete, isotopic fractionation that occurs during the chemical reaction will contribute to the error. The completeness of conversion to C≡O may be determined by comparing the integrated ion currents to known standards. The ability to quantitatively convert many different molecules to C≡O and determine the oxygen isotope ratio on-line should provide a practical method of determining many nucleophile KIEs. While this method was applicable to ADA, it could not be used for RNase P since the hydrolysis product contains numerous O atoms, preventing the analysis at natural abundance.

For the RNase P reaction we sought a method that would permit the same instrument to be used to determine the $^{18}O/^{16}O$ ratio in water and in the tRNA product. Since tRNA is too large to analyze directly, the reacted phosphate was isolated by digestion of the product with ribonuclease and isolation of the 5′-phosphate as guanosine 3′,5′-bisphosphate (pGp). By knowing the $^{18}k_{nuc}$ for the ADA reaction, it is possible to use the isotopic composition of the inosine generated by the hydrolysis of adenosine. This protocol hopes to limit the instrumental bias by using the same instrument, if not the same analyte, to determine both the water and product isotope ratios. The development of electrospray and MALDI ionization techniques has made it possible to determine isotope ratios with a precision of better than 0.5% in relatively large biological molecules ranging from amino acids (*40*) to cofactors and nucleotides (*27*). This approach was utilized to determine the RNase P $^{18}k_{nuc}$ according to eq 3 (derived from eqs 1 and 2a).

$$^{18}k_{nuc}(\text{RNase P}) = \{(6\text{-}^{18}O)\text{inosine}/(6\text{-}^{16}O)\text{inosine}\}/(^{18}k_{nuc}(\text{ADA}))/\{[(^{18}O)\text{pGp}]/[(^{16}O)\text{pGp}]\} \quad (3)$$

An alternative approach used the standard method of determining $H_2{}^{18}O/H_2{}^{16}O$ by CO_2 equilibration (*41*, *42*).

Success in this regard was reported in the determination of the isotope effect on hydrolysis of thymidine 5′-*p*-nitrophenyl monophosphate (T5PNP) (*27*). The application of this methodology, however, requires the recognition of the potential different instrumental biases and application of the best procedures to detect and minimize this source of possible systematic error. Quadrupole mass spectrometers due to their mass granularity have the potential to generate systematic errors in isotope ratio measurements (*43*). From comparison with predicted ratios from natural abundance isotopes, we found that the best method to eliminate this source of inaccuracy is to fit the limited range mass profile scan as shown in Figure 2B,C, assuming a sequence of identically shaped peaks (see below).

Mg^{2+}-Catalyzed T5PNP Hydrolysis. T5PNP, $MgCl_2$, and Tris were from Sigma, and 3-chloroquinuclidine (3ClQ) was from Aldrich. Reactions containing 0.25 mM T5PNP were monitored for accumulation of the *p*-nitrophenolate product using absorbance at 400 nm as measured by a Beckman 640DU spectrophotometer. Mg−OH concentration was varied by adjusting both the [$MgCl_2$] and pH of the reaction, and [Mg−OH] was calculated on the assumption of octahedral coordination of water and a pK_a of 11.4 (*44*). Reactions with 3ClQ were performed at pH 8.7 using 3ClQ as an intrinsic buffer. Pseudo-first-order rate constants were determined by the initial rates method (*45*) with less than 1% of the reaction completed. Second-order rate constants were determined by plotting pseudo-first-order rate constant versus nucleophile concentration. All data were analyzed using Kaleidagraph.

Reactions for determination of $^{18}k_{nuc}$ for Mg^{2+}-catalyzed T5PNP hydrolysis contained 0.3 M $MgCl_2$, 50 mM Tris (pH 9.1), and 5 mM T5PNP in ∼50% $H_2{}^{18}O$. The contribution of each solute to the mass of the reaction mixture was accounted for to aid in the calculation of the subsequent dilution (see below). Reactions were placed in flame-sealed glass ampules and incubated at 37 °C in a dry incubator for 65 days, at which point 4−5% of the reaction was complete. To assess the solvent $^{18}O/^{16}O$ ratio of enriched samples by isotope ratio mass spectrometry requires that they be accurately diluted; consequently, 100 μL aliquots were added to a 100 mL volumetric flask containing 10 mL of diluent (natural abundance ^{18}O) water. The mass of the aliquot was measured on a Mettler AG104 scale. The flask was then filled to the 100 mL line, and the mass of the 99.9 mL of diluent water was determined from the density of water at the measured temperature. Aliquots of the diluted reaction solutions and the diluent water were sealed by fire-sealing in glass ampules, and the ^{18}O content was analyzed by IR-MS (Iso-analytical Ltd.). The ^{18}O mole fraction of the reactant was then calculated iteratively from the equation

$$f_r = \frac{m_f f_f/M_f - m_d f_d/M_d}{m_r/M_r} \quad (4)$$

where f_r is the ^{18}O mole fraction for the reactant, m_f, M_f, and f_f are the mass, average molecular weight, and ^{18}O mole fraction of the final diluted mixture, m_d, M_d, and f_d are the mass, average molecular weight, and ^{18}O mole fraction of the diluent, and m_r and M_r are the mass and average molecular weight of the reaction aliquot. The reactant $^{18}O/^{16}O$ ratio was calculated directly from the mole fraction.

ESI-QMS measurements of pGp, adenosine, and TMP were performed using a Finnigan TSQ instrument in negative ion mode. Samples were injected by direct infusion at a rate of 10 μL/min. Samples were analyzed by both single ion monitoring (SIM) and scan data acquisition (scan). Data for both types of acquisitions were averaged over >200 data points. In all cases, a blank acquisition consisting of solvent only was subtracted from the sample acquisitions.

TMP samples were resuspended in methanol−water (50:50) to a concentration of ∼50 μM. Scan acquisition covered a range of m/z = 318−328 in 1 s with 10 points per m/z unit. The isotope ratio was calculated from the relative intensities m/z = 321 and 323. This ratio was corrected for both the natural abundance of ^{18}O, ^{13}C, ^{15}N, and ^{2}H and excess enrichment of ^{18}O due to the slow exchange of solvent into the thymine base or potentially due to Mg-catalyzed exchange into phosphate, determined from the relative intensities of m/z = 323 and 325. The corrected 323 u intensity is computed by subtracting the intensity of the 321 u peak multiplied by the observed 325 u/323 u ratio.

Isotope ratios from data procured in scan mode were determined by fitting the data to an equation describing the sum of five chromatographic peaks using SigmaPlot. Equation 5 describes the function for a single peak where B is

$$y = B + A\left(\frac{1}{1+e^{-(x-x_c+w_{1/2})/w_2}}\right)\left(1-\frac{1}{1+e^{-(x-x_c+w_{1/2})/w_3}}\right) \quad (5)$$

the baseline value, A is the amplitude of the peak, x_c is the mass center for the peak, $w_{1/2}$ is the peak width at one-half the height, and w_2 and w_3 are correction factors for the leading and trailing edges of the peak, respectively. This function was chosen for its ability to model leading and trailing peaks. For the equation describing the sum of five peaks, B was determined before fitting from the lowest intensity values observed in the mass range, and only parameter A was allowed to vary between the peaks under the assumption that changes in peak shape would be negligible. Excellent fits to this equation (R^2 > 0.999) support this assumption.

Ribonuclease P. Escherichia coli RNase P and pre-$tRNA^{Asp}$ from *Bacillus subtilis* (pre-tRNA) were synthesized by runoff in vitro transcription as described previously (*46*) using pEcRNAP and pDW152, respectively, with the exception that transcription reactions were scaled up to a 2 mL volume. Reactions contained 1 M NaCl (Sigma), 25 mM $MgCl_2$ (Sigma), 50 mM buffer, 3 mM adenosine, 2−5 nmol of RNase P, 30−50 nmol of pre-tRNA, and ∼50% $H_2{}^{18}O$ in a 500 mL total volume. Reactions run at pH 6 used MES (Sigma) as the buffer, and pH 8 reactions used Tris (Sigma). Prior to reaction initiation, RNase P and pre-tRNA were heated to 95 °C for 3 min and then cooled to 37 °C for 2 min separately under reaction conditions except for the absence of $MgCl_2$. $MgCl_2$ was then added, and the RNAs were incubated for an additional 20 min at 37 °C before the reaction was initiated by combining enzyme and substrate. After the reaction was initiated, a 100 mL aliquot (out of 500 mL) was removed and added to a tube containing dried calf intestinal ADA (0.5 mL of 0.1 unit/mL, from Sigma). Both the RNase P and the ADA reactions were layered with mineral oil to prevent exchange of the ^{18}O-enriched water with atmospheric moisture. ADA reactions were incubated

for 1 h at 37 °C and then stored at −80 °C. RNase P reactions were incubated for either 8 h (pH 8) or 16 h (pH 6) at 37 °C. Following incubation, the mineral oil layer was removed by extraction with chloroform, and the RNA was ethanol precipitated.

Mature tRNA was purified from the RNase P reactions by ethanol precipitation followed by denaturing polyacrylamide gel electrophoresis as described previously (*46*). The recovered tRNA was resuspended in 100 mL of 50 mM sodium acetate, pH 4.5. Seventeen units of ribonuclease T_2 was added, and the reaction was incubated overnight at 37 °C to digest the tRNA to mononucleotides. The reacted 5′-phosphate, in the form of pGp, was purified from the 3′-nucleotide monophosphates by reverse-phase HPLC. The reaction mixture was injected onto a C_{18} reverse-phase column (300 mm × 3.9 mm, 10 μm packing, from Phenomenex), and the nucleotides were eluted isocratically using 50 mM diisopropylethylamine (Aldrich) and 1% acetic acid in water (pH 4.3) as the mobile phase. Fractions containing pGp were collected by hand, desalted using multiple rounds of lyophilization, and resuspended in water. For ADA reactions, the mineral oil layer was removed by chloroform extraction after thawing. The remaining mixture was then loaded onto the reverse-phase column, and the inosine was purified and desalted as described above for pGp.

The pGp samples for mass spectrometric analysis were resuspended in methanol−water−acetic acid (50:50:0.1) to a concentration of ∼100 μM. SIM acquisitions were performed with a 0.1 *m*/*z* window centered at *m*/*z* = 440.03, 442.03, 443.03, 444.03 445.03, 446.03, and 447.03. Scan acquisitions covered a range of *m*/*z* = 439−449 with 1 s scan times and either 10 or 25 points per *m*/*z* unit. The isotope ratio was calculated from the relative intensities at *m*/*z* = 442 and 444. The ratio was corrected for the unenriched intensity at *m*/*z* = 444 due to the natural abundance of ^{18}O, ^{13}C, ^{15}N, and ^{2}H. This intensity was calculated from the known natural abundance of these isotopes.

Both the SIM and scan methods for measuring isotope ratios were utilized for determining $^{18}k_{nuc}$ for RNase P catalyzed phosphodiester hydrolysis. When both methods were used to analyze the same reaction, the difference in the calculated isotope effect was only 0.002, while the standard deviation of $^{18}k_{nuc}$ for multiple reactions was ∼0.01. Similarly, eliminating the values determined using the SIM method did not substantially alter the average $^{18}k_{nuc}$. These results indicate that, for the RNase P reactions, the uncertainty introduced by pooling values determined using both the SIM and scan methods is small compared to the overall uncertainty in the measurement. For this reason, both the SIM and scan data were used to compile the RNase P isotope effects.

Adenosine Deaminase. The $^{18}k_{nuc}$ for the ADA reaction was measured at pH 8 in the absence and presence of 25 mM $MgCl_2$ and 1 M NaCl to mimic the conditions of the RNase P reactions. Reaction mixtures for both conditions contained 30 mM adenosine and 10 units of ADA and were 5 mL in volume. Aliquots (1 mL) were removed for determination of solvent ^{18}O content and placed in flame-sealed glass ampules for storage. Reactions were incubated for either 2 h at 24 °C (no $MgCl_2$ or NaCl) or 4 h at 37 °C (+$MgCl_2$ and NaCl). Reaction progress was monitored by A_{280}/A_{260} on a Beckman 640DU spectrophotometer.

Table 1: Effect of Mg^{2+} on Second-Order Rate Constants for Hydroxide- and 3-Chloroquinuclidine-Catalyzed T5PNP Cleavage

	k ($\times 10^{-5}$ min^{-1} M^{-1})
hydroxide	4.3 ± 0.1
hydroxide/0.3 M Mg^{2+}	450 ± 50
3-chloroquinuclidine	0.25 ± 0.01
3-chloroquinuclidine/0.3 M Mg^{2+}	0.25 ± 0.08

The hypoxanthine base of the inosine product was removed from the ribose moiety by nucleoside phosphorylase catalyzed arsenolysis. Ten units of nucleoside phosphorylase and 80 μL of 1 M Na_2HAsO_4 were added, and reactions were further incubated for either 16 h (no $MgCl_2$ or NaCl) or 36 h (+$MgCl_2$ and NaCl). Arsenate was added to allow quantitative conversion to ribose and hypoxanthine (*47*), and the reaction progress was monitored by A_{280}/A_{260}. The volume was reduced to <500 μL using dry nitrogen, the resulting mixture was cooled with a wet ice slurry, and the hypoxanthine precipitate was pelleted by centrifugation. After the supernatant was removed, hypoxanthine was purified by several recrystallization steps and dried in an evacuated desiccator over P_2O_5 at 80 °C. Analyses of hypoxanthine and water samples for ^{18}O content were performed by Dr. John Morrison at Micromass (now GV) Instruments. Briefly, all oxygen was converted to carbon monoxide in a carbon reduction reaction oven of a thermal conversion elemental analyzer, and the carbon monoxide was analyzed by continuous-flow IRMS (*48*). This method was applied to the solvent without prior treatment. For the inosine, the hypoxanthine base was first removed from the ribose as described above to eliminate the contribution of the ribose oxygen atoms to the measured $^{18}O/^{16}O$ ratio.

For determination of the $^{18}O/^{16}O$ ratio by ESI-QMS the inosine samples were resuspended in methanol−water−ammonium hydroxide (50:50:0.1) to a concentration of ∼120 μM. SIM acquisitions were performed with a 0.1 *m*/*z* window centered at 265.04, 267.04, 268.04 269.04 270.04, 271.04, and 272.04. Scan acquisitions covered a range of *m*/*z* = 264−274 in 1 s with either 10 or 25 points per *m*/*z* unit. The isotope ratio was calculated from the relative intensities at *m*/*z* = 267 and 269. The ratio was corrected for the unenriched intensity at *m*/*z* = 269 as described above.

RESULTS

Mg^{2+}-Catalyzed T5PNP Hydrolysis. Metal ion catalysis of phosphodiester hydrolysis has been previously examined (*26*, *49*−*51*). The mechanisms discussed in these studies commonly invoke nucleophilic activation by metal coordination, and this model has been confirmed for organometallic complexes of Ir^{3+} and Cu^{2+} (*49*, *50*). However, these investigations focused on transition metal complexes and lanthanide metals, and less is known regarding catalysis of aqueous phosphodiester hydrolysis by Mg^{2+}, the most common biological cofactor.

To better understand the means by which Mg^{2+} can promote phosphodiester reactions, we examined the ability of Mg^{2+} to catalyze the hydrolysis of T5PNP (Figure 1B). Table 1 shows the second-order rate constants for hydroxide- and 3-chloroquinuclidine- (3ClQ-) catalyzed T5PNP cleavage

Table 2: ^{18}O Isotope Effects on the Nucleophile ($^{18}k_{Nuc}$) for Enzyme-Catalyzed Adenosine Deamination and for Mg^{2+}-, Hydroxide-, and Ribozyme-Catalyzed Phosphodiester Hydrolysis

	$^{18}k_{nuc}$	*N*
T5PNP hydroxide	1.068 ± 0.007	9
T5PNP hydroxide/Mg^{2+}	1.027 ± 0.013	3
ribonuclease P, pH 8	1.015 ± 0.011	3
ribonuclease P, pH 6	1.030 ± 0.012	5
adenosine deaminase	0.988 ± 0.001	3
adenosine deaminase[a] (RNase P conditions)	0.986 ± 0.001	3

[a] 1 M NaCl and 25 mM $MgCl_2$.

in the presence and absence of 0.3 M $MgCl_2$. Because 3ClQ is a tertiary amine nucleophile, any Mg^{2+} coordination of 3ClQ will occur through the single lone pair of electrons and effectively eliminate the nucleophilic capability of the coordinated amine. Thus, any Mg^{2+} catalysis observed for this reaction would result from interactions between the metal ion and the nonnucleophilic segments of the transition state. We find that Mg^{2+} catalyzes the hydrolysis of T5PNP over 10^3-fold for the hydroxide nucleophile but no catalysis occurs for the 3ClQ reaction. These results suggest that Mg^{2+} catalysis of T5PNP hydrolysis results primarily or exclusively from interactions with the nucleophile.

To further examine the involvement of Mg^{2+} in nucleophilic activation, we determined the dependence of T5PNP cleavage on the concentration of divalent magnesium−hydroxide complexes (Mg−OH). Figure 3 demonstrates that T5PNP cleavage rate is linearly dependent on [Mg−OH], suggesting a single metal ion participates in catalysis, and that Mg−OH is the catalytic species. The slope indicates that the second-order rate constant for Mg−OH displacement of the *p*-nitrophenolate leaving group is $(2.0 \pm 0.1) \times 10^{-4}$ M^{-1} min^{-1}. This value is 5-fold greater than the second-order rate constant for the hydroxide-catalyzed reaction in the absence of Mg^{2+}, despite the fact that the pK_a for deprotonation of water complexed to magnesium to yield Mg−OH is 11.4 (*44*), much less than the value for deprotonation of water to generate hydroxide (15.7). Assuming a β_{nuc} for attack by oxyanions on phosphodiester centers of 0.3 (*4*), the expected second-order rate constant for Mg−OH-catalyzed T5PNP hydrolysis is only 2.2×10^{-6}. Thus, the catalysis by Mg^{2+} on T5PNP cleavage by hydroxide is 100-fold greater than can be explained by lowering the pK_a of the coordinated water alone, indicating that the nucleophile is activated by one or more additional mechanisms.

To better understand whether Mg^{2+} coordination of the water nucleophile is occurring in the transition state, we determined $^{18}k_{nuc}$ for the T5PNP hydrolysis reaction in the presence of Mg^{2+}. Such a direct interaction necessarily imparts a stiffer bonding environment on the bound water relative to solution. Thus, metal coordination is anticipated to result in an inverse contribution and, thus, a lower $^{18}k_{nuc}$ for the metal ion catalyzed reaction compared to that catalyzed by hydroxide alone. As shown in Table 2, the measured $^{18}k_{nuc}$ for Mg^{2+}-catalyzed T5PNP hydrolysis is 1.027 ± 0.013. The normal isotope effect indicates that nucleophilic attack occurs during formation of the rate-limiting transition state. Importantly, the magnitude of the observed effect is 0.04 less than the $^{18}k_{nuc}$ of 1.068 observed for the hydroxide-catalyzed reaction (*27*), consistent with stiffer bonding to the nucleophile as predicted by models invoking direct coordination of the hydroxide nucleophile by Mg^{2+}.

Isotope Incorporation Studies of the RNase P Catalyzed Reaction. To extend these analyses to RNA and protein phosphodiesterases, we examined the mechanism of nucleophilic activation by the RNase P ribozyme, a Mg^{2+}-dependent ribonuclease in which metal ion catalysis is proposed to activate the solvent nucleophile. However, interpretation of HAIE in enzymatic systems can be challenging when a step other than the chemical reaction is rate limiting for production of the enzyme−product complex. In such circumstances, this step represents a "commitment to catalysis" (*22*, *52*), and these commitments can occur in either the forward or reverse direction. Forward commitments can often be ameliorated by reducing the rate constant of the chemical step, while reverse commitments may be reduced if the affinity for the product can be decreased. The best test for the existence of a reverse commitment is to assess the reversibility of the chemical step. If the chemical reaction is irreversible, the reverse commitment will be zero by definition.

To test the reversibility of the RNase P catalyzed reaction, we assayed the incorporation of ^{18}O into the scissile phosphate in 50% ^{18}O water. If the RNase P chemical step is *irreversible*, the hydrolysis reaction occurs only once and a *single* solvent ^{18}O could be incorporated into the scissile phosphate (Figure 2A and Figure 5). In contrast, a readily reversible chemical step with a nonzero reverse commitment will result in multiple hydrolysis and ligation events before the products are released. Thus, for a *reversible* chemical step, the incorporation of *multiple* ^{18}O atoms into the scissile phosphate is expected, while the incorporation of a *single* ^{18}O atom is strong evidence for the irreversibility of the reaction.

Because the mass of the tRNA product is too large for quantitative analysis by ESI-QMS, the scissile phosphate was isolated from this macromolecule as the 5′-phosphate of pGp as described in Materials and Methods. Figure 2B depicts the control negative ion ESI-QMS mass spectrum of enzymatically synthesized pGp. The major peak at m/z = 442 represents ion intensity for the pGp monoisotopic mass (M) of the monoanion. The substantial peak observed at M + 1 corresponds to the natural abundance of ^{13}C, ^{15}N, ^{17}O, and ^{2}H; similarly, the M + 2 peak corresponds to the natural abundance of ^{18}O present in the pGp.

Figure 2C shows the mass spectrum for pGp containing the scissile phosphate of an RNase P catalyzed reaction in 50% ^{18}O water. The peak at m/z 442 is again very strong, but in this spectrum the M + 2 peak, resulting from ^{18}O incorporation during hydrolysis, is roughly equal in magnitude. The peaks at M + 1 and M + 3 correspond to the natural abundance ^{13}C, ^{15}N, ^{17}O, and ^{2}H for the products with ^{16}O and ^{18}O incorporated into the phosphate, respectively. Importantly, the intensity of the M + 4 peak relative to the M + 2 peak is indistinguishable from the intensity of the M + 2 peak relative to the M peak from the control spectrum. This observation indicates that the M + 4 peak corresponds only to the natural abundance of ^{18}O in pGp molecules where a single ^{18}O has been incorporated into the scissile phosphate. Together, these results demonstrate that the RNase P chemical step is irreversible and that there is no significant reverse commitment.

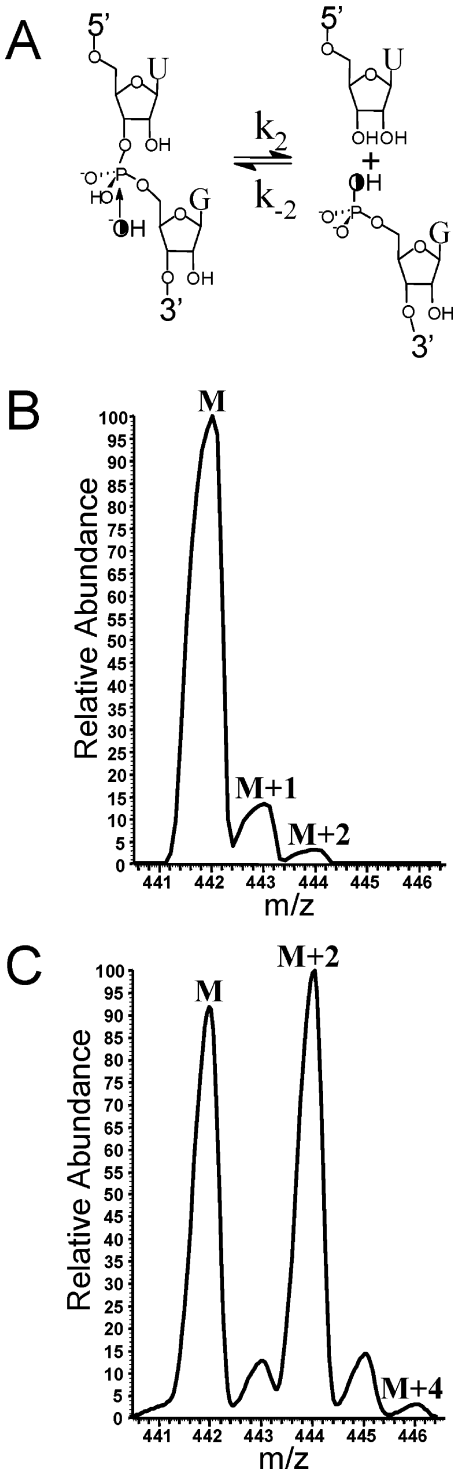

FIGURE 2: Incorporation of ^{18}O into the scissile phosphate of RNase P catalyzed phosphodiester hydrolysis. (A) Scheme for ^{18}O incorporation during the hydrolysis step of RNase P catalysis. The half-filled oxygen atom represents a solvent containing ~50% ^{18}O. (B) Mass spectrum of a pGp standard. A major peak exists at the monoisotopic mass of $m/z = 442$. M + 1 and M + 2 peaks represent pGp species containing natural abundance levels of ^{13}C, ^{15}N, ^{2}H, ^{17}O, and ^{18}O. (C) Mass spectrum of pGp containing the scissile phosphate from the RNase P catalyzed reaction. Major peaks occur at M and M + 2, representing incorporation of a ^{16}O and ^{18}O nucleophile, respectively. The peak at M + 4 corresponds to the natural abundance of ^{18}O for the 10 other oxygen atoms in pGp molecules with a single ^{18}O incorporated by hydrolysis.

Using ADA To Monitor Solvent $^{18}O/^{16}O$ Isotope Ratios. Analysis of HAIEs by the competitive method (*28*) requires the ability to measure isotope ratios with great precision. For the RNase P catalyzed reaction, ESI-QMS was used to measure the isotope ratio for the product (in the form of pGp). Determination of the substrate (solvent) isotope ratio presents unique challenges. Most often, these ratios are measured by exchange into CO_2 and subsequent analysis of CO_2 by IRMS. However, the high level of ^{18}O enrichment required for the ESI-QMS analysis precludes IRMS analysis. Previously, this obstacle was circumvented by diluting the reaction solution prior to CO_2 exchange (*27*). However, this technique requires precise knowledge of the contributions of the solutes to the mass of the solution. The high concentrations of RNase P and pre-tRNA in the RNase P reactions make this requirement difficult to achieve. For these reasons, solvent isotope ratios were monitored by a parallel ADA reaction. Because ADA incorporates a single solvent oxygen to form the inosine product (Figure 4), measuring the isotope ratio of the inosine, again using ESI-QMS, allows the determination of the isotopic content of the solvent as described in Materials and Methods. However, this strategy requires knowledge of the $^{18}k_{nuc}$ for ADA for use as a correction factor for calculation of the solution $^{18}O/^{16}O$ ratio (eq 3).

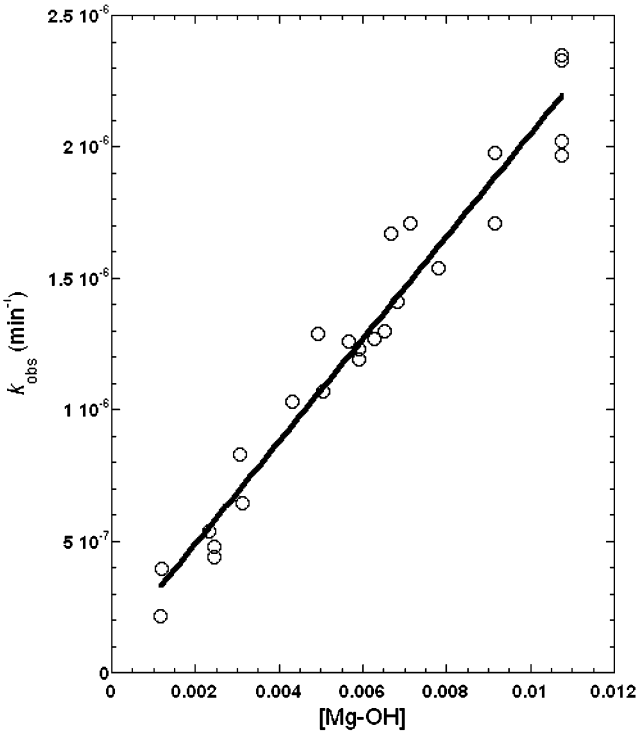

FIGURE 3: Linear dependence of the rate of T5PNP hydrolysis on the concentration of Mg−OH. The value of k_{obs} corresponds to the pseudo-first-order rate constant at each [Mg−OH]. [Mg−OH] was calculated on the assumption of octahedral coordination of water and a pK_a of 11.4 (*44*). The line is a fit of the data to a linear equation yielding a second-order rate constant of (2.0 ± 0.1) × 10^{-4} M^{-1} min^{-1}.

The $^{18}k_{nuc}$ for ADA was determined at natural abundance ^{18}O using IRMS to measure precursor and product isotope ratios. The $^{18}k_{nuc}$ for the ADA reaction was measured at pH 8 in the absence and presence of 25 mM $MgCl_2$ and 1 M NaCl (Table 1) to mimic the conditions of the RNase P reactions. The isotope effect was 0.988 ± 0.001 in the absence of $MgCl_2$ and NaCl and 0.986 ± 0.001 in the presence of $MgCl_2$ and NaCl. This latter value was used to

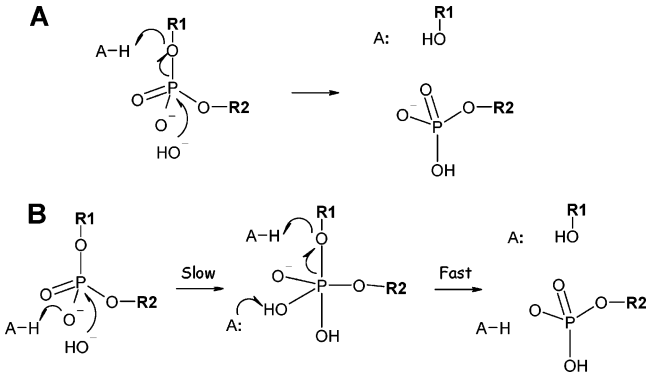

FIGURE 4: Possible mechanisms for Mg^{2+} RNase P catalyzed tRNA cleavage. (A) Concerted mechanism: Simultaneous bond formation and bond breakage. (B) Stepwise mechanism: Rate-limiting formation of a phosphorane intermediate, aided by protonation of a nonbridging oxygen atom, followed by rapid breakdown of the intermediate into products.

correct the measured $^{18}O/^{16}O$ isotope ratio in inosine, yielding the original isotope ratio in the solvent for the RNase P reactions.

$^{18}k_{nuc}$ for RNase P Catalyzed RNA Hydrolysis. With $^{18}k_{nuc}$ for the ADA reaction in hand, it was possible to determine the RNase P $^{18}k_{nuc}$ at pH 6 and 8 (Table 2). The reaction displays a normal (>1) $^{18}k_{nuc}$ equal to 1.030 ± 0.012 at pH 6 and 1.015 ± 0.011 at pH 8. A Student's *t* test indicates that the data sets for these two conditions represent distinct values between the 80% and 90% confidence levels. The pre-tRNA cleavage step for RNase P is 100-fold slower at pH 6 compared to pH 8 (*32*), substantially reducing any contribution of forward commitments to the observed isotope effect at this pH. Therefore, the $^{18}k_{nuc}$ measured at pH 6 is interpreted as the intrinsic isotope effect. The lower $^{18}k_{nuc}$ at pH 8 indicates that as the rate of the cleavage step increases, a second step in catalysis, upstream of cleavage, is partially contributing toward isotopic discrimination of the nucleophile. That is, the intrinsic isotope effect is reduced by a partial forward commitment for incorporation of the water "substrate".

If the data sets for the pH 6 and 8 reactions are reflecting the *same* value for $^{18}k_{nuc}$, the observed isotope effect is then 1.024 ± 0.013. Under this interpretation, $^{18}k_{nuc}$ remains constant over a 100-fold change in the rate of pre-tRNA cleavage, indicating that this value represents the intrinsic isotope effect. The intrinsic isotope effects assuming *either* distinct (1.030 ± 0.012, $n = 5$) *or* uniform (1.024 ± 0.013, $n = 8$) $^{18}k_{nuc}$ values at pH 6 and 8 are *both* greater than unity to greater than the 99% confidence level as determined by Student's *t* tests. For these reasons mechanistic interpretation of $^{18}k_{nuc}$ is best done using the pH 6 value; however, all interpretations made would be essentially identical using the combined average of the pH 6 and 8 trials.

The normal isotope effect again indicates that nucleophilic attack occurs in the rate-determining transition state for RNase P catalyzed phosphodiester hydrolysis. A comparison between the $^{18}k_{nuc}$ values for RNase P at pH 6 (1.030 ± 0.012) and hydroxide-catalyzed hydrolysis of a model phosphodiester (1.068 ± 0.007) reveals a significant reduction in the observed effect for the ribozyme reaction, similar to that observed for the Mg^{2+}-catalyzed reaction. This reduction reflects a stiffer bonding environment for the nucleophile in the transition state of RNase P catalyzed phosphodiester hydrolysis compared to the alkaline reaction, consistent with direct coordination of the nucleophilic water by an active site metal ion.

DISCUSSION

The value of the observed kinetic HAIE reflects both the fractionation of the isotopes for all equilibria prior to transition state formation and the kinetic effect of isotopic substitution. The KIE, in turn, is composed of two factors, the temperature-independent factor (TIF) and the temperature-dependent factor (TDF) (*53*). The TIF reflects the extent to which the isotopically labeled atom participates in reaction coordinate motion. This factor always favors the lighter isotope, producing normal contributions to the observed isotope effect. The TDF, in contrast, reflects the change in bonding the atom experiences upon going from the ground state to the transition state. Similarly, equilibrium HAIE correspond to the difference in bonding to the labeled atom between the reactants and the products. For both the TDF and equilibrium isotope effects, "stiffer" bonding to the labeled atom favors the heavier isotope (yielding inverse isotope effects), and "looser" bonding to the labeled atom favors the lighter isotope (yielding normal isotope effects). These principles provide a general framework for the interpretation of HAIE.

For nucleophile KIEs, bond formation to the nucleophile in the transition states results in inverse contributions from the TDF. However, this contribution is frequently overcome by contributions from the TIF, and so nucleophile KIEs are generally normal (*27*, *54*−*57*). Inverse nucleophile KIEs are possible in late transition states where bond formation is so advanced that the TDF is greater than the TIF (*54*, *58*). Additionally, if nucleophilic attack forms an intermediate in a stepwise mechanism, the observed isotope effect may be inverse if breakdown of the intermediate is rate determining. In the extreme case, where breakdown is completely rate determining, the observed $^{18}k_{nuc}$ represents the equilibrium isotope effect on intermediate formation. Thus, large inverse nucleophile isotope effects are interpreted to indicate stepwise mechanisms (*9*).

$^{18}k_{nuc}$ for the ADA-Catalyzed Reaction. The motivation for determining $^{18}k_{nuc}$ for ADA was to monitor the $^{18}O/^{16}O$ ratio of the solvent for complex enzyme reaction mixtures, and the results presented here indicate that ADA can be used to monitor solvent ^{18}O content under a range of reaction conditions. The isotope effect was determined at pH 8 under two significantly different salt concentrations, with and without 1 M NaCl and 25 mM $MgCl_2$ in addition to 10 mM Tris, pH 8. The values for $^{18}k_{nuc}$ under these conditions were 0.986 and 0.988, respectively, which are quite similar considering the significantly different ionic strengths. Additionally, V_{max}/K_M, the kinetic parameter probed by the competitive method, plateaus from pH 6 to pH 8.5 (*59*). These properties indicate that the ADA reaction can be used as a probe for solvent ^{18}O content under a variety of conditions.

Although the ADA isotope effect was determined as a correction factor, it also provides useful information regarding the mechanism of nucleophilic activation. As described above, the inverse nature of the $^{18}k_{nuc}$ for ADA is unusual,

and two aspects of the proposed reaction mechanism could contribute to the observed inverse effect. ^{18}O EIEs for addition to carbon double bonds are inverse and predicted to be 0.96[2] for the formation of the proposed tetrahedral intermediate (*60*). If cleavage of the C−N bond were completely rate determining, it would impose a large reverse commitment on the preceding addition of water and $^{18}(V/K_{H_2O})$ would approach the inverse EIE of 0.96. Thus, the measured value of 0.986 is inconsistent with C−N bond cleavage being completely rate determining. Under similar reaction conditions, Weiss et al. used the primary $^{15}(V/K_{adenosine})$ to determine the reverse commitment factor for C−O bond formation to be 1/1.4 (*61*). Using the estimated ^{18}O EIE of 0.96, the $^{18}k_{nuc}$ for addition of the Zn^{2+}-bound water (or hydroxide) to C6 would be 1.0042.[3] A larger normal value, e.g., similar to those measured for the double bond hydration reactions (*62*−*64*), would result in a normal observed $^{18}(V/K_{H_2O})$. This reduction in the intrinsic $^{18}k_{nuc}$ can be attributed to coordination of the nucleophilic water to the divalent metal ion and is consistent with the known inverse EIE on water coordination to divalent metal ions (*65*). A second possibility is that the inverse EIE on coordination of water by Zn^{2+} could potentially be the sole contributor to the observed $^{18}k_{nuc}$ if the binding of adenosine were to trap the nucleophilic Zn^{2+} hydroxide, resulting in a large forward commitment. Such trapping of Zn^{2+}-coordinated water is predicted by the crystal structure of murine ADA in complex with 6-hydroxy-1,6-dihydropurine ribonucleoside (*66*). However, the large forward commitment is not consistent with the observed normal $^{15}(V/K_{adenosine})$ (*61*).

Mechanism of Mg^{2+}-Catalyzed Phosphodiester Hydrolysis. As described above, previous nonenzymatic studies regarding catalysis of phosphodiester hydrolysis by metal ions have not included Mg^{2+}, the most common biological cofactor. However, catalysis of phosphomonoester bond cleavage, including hydrolysis by Mg^{2+}, has been well characterized (*67*, *68*). This work revealed that the mechanisms of Mg^{2+} catalysis include (i) increasing the local hydroxide concentration by lowering the pK_a of coordinated water molecules, (ii) inducing an intramolecular reaction by simultaneously interacting with the phosphomonoester and the nucleophile in the transition state, and (iii) stabilizing the negative charge that builds up on the leaving group. Multiple metal ions acting simultaneously were required to fulfill these various roles. Metal ions were not found to alter the highly dissociative transition state of phosphomonoester hydrolysis, indicating that Lewis acid catalysis was not a significant factor.

The kinetic data presented here show that Mg^{2+} catalyzes displacement of nitrophenol from phosphodiesters primarily, if not solely, through interactions with the water nucleophile. Additionally, the linear dependence of the rate of T5PNP cleavage on [Mg−OH] indicates that the metal−hydroxide complex is the catalytic species. This interpretation is favored over the kinetically equivalent possibility that T5PNP cleavage is dependent separately on [Mg^{2+}] and [HO^-] because, in this latter case, Mg^{2+} catalysis would also be expected when 3ClQ is the nucleophile. The simplest mechanism for Mg−OH catalysis is for the metal-coordinated hydroxide to act directly as the nucleophile. This mechanism is consistent with the mechanism of hydroxide-catalyzed T5PNP hydrolysis, where hydroxide is also the nucleophile (*27*). Nucleophilic activation arises from the lowered pK_a of the metal−water complex (to 11.4 compared to 15.7 for uncoordinated water) increasing the available concentration of the more reactive hydroxide. Interestingly, the second-order rate constant for Mg−OH catalysis is ∼100-fold greater than expected if nucleophilic activation occurred only through increasing the hydroxide concentration. This additional catalysis likely results from the induced intramolecularity of Mg^{2+} interacting simultaneously with a nonbridging phosphate oxygen atom and the nucleophile. This level of catalysis from induced intramolecularity is, in fact, the same as observed for phosphomonoester hydrolysis (*68*).

Although the mechanisms of nucleophilic activation are very similar between Mg^{2+}-catalyzed phosphodiester and phosphomonoester hydrolysis, some mechanistic differences are observed. The phosphomonoester mechanism involves a second metal ion that contributes to catalysis by stabilizing the developing negative charge on the leaving group (*67*). In contrast, the linear dependence on [Mg−OH] suggests that only a single metal ion is involved in phosphodiester hydrolysis. Additionally, because Mg^{2+} displays no effect on the 3ClQ reaction, leaving group stabilization cannot play a major role in catalysis. The fact that phosphomonoesters have two negatively charged nonbridging oxygens available for coordinating metal ions compared to only one for phosphodiesters may explain the additional Mg^{2+} in nonenzymatic metal-catalyzed phosphomonoester hydrolysis.

The $^{18}k_{nuc}$ of 1.027 ± 0.013 observed for the Mg^{2+} catalyzed contrasts sharply with $^{18}k_{nuc}$ for phosphodiester hydrolysis catalyzed by a dinuclear Co^{3+} complex (0.937 ± 0.002) (*9*). The large inverse effect for the Co^{3+} complex reaction demonstrates a stepwise mechanism with equilibrium formation of a phosphorane intermediate and rate-limiting expulsion of the leaving group. This conclusion is further supported by analysis of nucleophile isotope effects for hydrolysis of a monoester by the dinuclear cobalt complex in which a normal, small $^{18}k_{nuc}$ is observed (1.013) together with an appreciable leaving group isotope effect demonstrating a concerted mechanism (A. C. Hengge, personal communication). Similarly, the normal $^{18}k_{nuc}$ observed for Mg^{2+} catalysis clearly demonstrates that nucleophilic attack occurs in the rate-limiting step. Therefore, the reaction must occur by either a concerted mechanism or a stepwise mechanism with rate-limiting formation of the phosphorane intermediate (Figure 5).

Although both mechanisms depicted in Figure 5 are consistent with the observed HAIE, the majority of evidence favors the concerted mechanism. All metal-catalyzed phosphodiester hydrolysis reactions thus far examined display isotope effects on the leaving group (*9*, *26*, *50*), indicating that these reactions occur by either a concerted mechanism or a stepwise one with rate-limiting bond cleavage to the leaving group. The simplest interpretation for the observation of both leaving group and nucleophile isotope effects for nonenzymatic metal-catalyzed phosphodiester hydrolyses is that they proceed by concerted mechanisms. The notable

[2] The value of 0.96 comes from the reciprocal of the fractionation factor for malate (1.033) and assuming that replacing a H with N will increase the fractionation factor by 1.008.

[3] This value is calculated using the standard commitment factor equation $^{18}k_{obs} = (^{18}k_{nuc} + c_r{}^{18}K_{eq})/(1 + c_r)$.

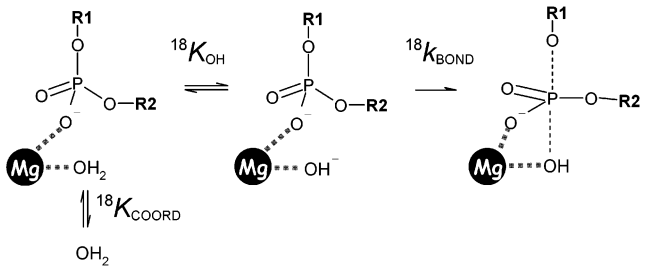

FIGURE 5: Effects of direct coordination by Mg^{2+} on the observed $^{18}k_{nuc}$. Coordination of water by Mg^{2+} exhibits an inverse (0.99) isotope effect ($^{18}K_{coord}$) (*70*). Magnesium will also perturb the equilibrium isotope effect on deprotonation of water to form hydroxide ($^{18}K_{OH}$), resulting in a similar inverse shift in the observed effect. It is also possible that metal ion interactions can alter the intrinsic kinetic isotope effect for bond formation ($^{18}k_{bond}$); however, metal ion coordination does not appear to alter the transition state for monoester hydrolysis.

exception is the stepwise mechanism observed for catalysis by the dinuclear Co^{3+} complex described above. However, this mechanism involved rapidly reversible formation of the phosphorane intermediate and rate-limiting expulsion of the leaving group. Likewise, the stepwise mechanism proposed for intramolecular cleavage of RNA also entails rate-limiting expulsion of the leaving group (*8*, *69*). Therefore, the normal $^{18}k_{nuc}$ of the Mg^{2+}-catalyzed reactions is inconsistent with the stepwise mechanisms observed for phosphodiester cleavage but consistent with the concerted mechanism (Figure 5).

The substantial decrease in $^{18}k_{nuc}$ observed for Mg^{2+}-catalyzed T5PNP hydrolysis compared to the hydroxide-catalyzed reaction (1.027 versus 1.068) is consistent with stiffer bonding to the nucleophile in the Mg^{2+}-catalyzed transition state attack by a metal-coordinated hydroxide. The nearly 0.04 inverse shift likely results from multiple influences of Mg^{2+} on the observed $^{18}k_{nuc}$ (Figure 5). Coordination of water by Mg^{2+} contributes a 0.99 EIE ($^{18}K_{coord}$) (*70*). Metal coordination can further reduce the observed isotope effect by lowering the 1.04 equilibrium isotope effect on deprotonation of water to form hydroxide ($^{18}K_{OH}$) (*71*). For the extremely strong interaction between water and Co^{3+} the $^{18}K_{OH}$ is reduced to 1.01 (*72*). When combined, $^{18}K_{coord}$ and $^{18}K_{OH}$ could conceivably account for the entire decrease in $^{18}k_{nuc}$ observed between the Mg^{2+}- and hydroxide-catalyzed reactions. However, the coordination of water by Mg^{2+} is much weaker than by Co^{3+}. Therefore, the reduction in the deprotonation isotope effect incurred by Mg^{2+} coordination is expected to be significantly less. Thus, Mg^{2+} may also affect the kinetic isotope effect on bond formation ($^{18}k_{bond}$). One possibility is that the "induced intramolecularity" provided by Mg^{2+} reduces the reaction coordinate motion experienced by the nucleophile compared to the hydroxide-catalyzed reaction, reducing the TIF component of the isotope effect. Alternatively, the reduced nucleophilicity of Mg−OH compared to hydroxide may require increased bond formation to expel the leaving group. This stiffer bonding in the transition state would result in a lower TDF contribution to the isotope effect.

Analysis of the RNase P Kinetic and Chemical Mechanisms. The results presented here help to refine the kinetic scheme for RNase P (*3*) by assessing the reversibility of the RNase P catalyzed reaction and by detecting a possible solvent trapping step upstream of pre-tRNA cleavage. The incorporation of a single ^{18}O atom into the scissile phosphate during RNase P catalyzed pre-tRNA hydrolysis in ^{18}O-enriched water strongly indicates that the reaction is irreversible. This result is distinct from several ATP hydrolases (*73*, *74*) but identical to the observed mechanism for the site-specific protein phosphodiesterase RNase III (*75*).

Statistical analysis of the pH 6 and 8 $^{18}k_{nuc}$ values for the RNase P catalyzed reaction suggests that the magnitude of the observed isotope effect decreases as pH increases. This observation would be consistent with the introduction of a forward commitment to catalysis with an increase in the rate of the cleavage step. Such a forward commitment would require that the solvent nucleophile be sequestered and unable to exchange with bulk solvent by an event upstream of the cleavage step. This event could include binding of the pre-tRNA substrate or a conformational change.

Models for ribozyme-catalyzed intermolecular phosphodiester cleavage uniformly propose concerted S_N2 mechanisms (*34*, *76*, *77*). These proposals are based on the S_N2 mechanism representing the simplest explanation for observed inversion of the stereochemical configuration at P for these reactions (*78*−*80*). Concerted mechanisms have also been proposed for protein enzymes based on inversion of configuration (*81*, *82*), and this interpretation is supported by the concerted mechanisms observed for the nonenzymatic reactions (*4*, *83*). However, the observed inversion of configuration for RNase A catalyzed cleavage (*84*) has not resolved the debate of whether this reaction proceeds by a concerted or stepwise reaction (*7*, *10*).

Additionally, recent work with protein enzymes indicates that these assumptions require testing on a case by case basis. The crystal structure of the phosphoglucomutase enzyme−intermediate complex suggests that enzyme active sites can shift the equilibrium between phosphate and the phosphorane intermediate to favor formation of the phosphorane even for normally dissociative phosphomonoester bond cleavage (*12*). The authors propose that this shift could be achieved by (i) minimizing the entropy of the enzyme−substrate complex to reduce the additional loss in entropy upon formation of the phosphorane compared to aqueous solution and (ii) compensating for enthalpic cost of the weak apical bonds in the phosphorane by forming multiple strong interactions with the apical oxygen atoms. Because entropy minimization of the enzyme−substrate complex through a preorganized active site and the ability to form multiple, simultaneous interactions with the substrate are hallmarks of all enzyme-catalyzed reactions, formation of a phosphorane intermediate remains a formal possibility for any enzyme-catalyzed phosphoryl transfer. Indeed, stepwise mechanisms have been proposed for the small ribozymes (*69*, *85*), which utilize an intramolecular 2′-OH nucleophile in a mechanism analogous to that of RNase A. Additionally, there is recent evidence from crystallographic analysis of the structure of fructose-1,6-bisphosphatase for formation of metaphosphate as opposed to the expected concerted mechanism of nonenzymatic reactions (*86*). Importantly, the bonding environment for the nucleophile is dramatically different for these different mechanisms, and this perspective on $^{18}k_{nuc}$ would provide a key test of these conclusions.

The normal $^{18}k_{nuc}$ observed for RNase P catalyzed pre-tRNA hydrolysis (1.030 ± 0.012) again demonstrates that nucleophilic attack occurs in the rate-limiting transition state

as it did for Mg^{2+}-catalyzed T5PNP hydrolysis. Therefore, RNase P must also proceed by either a concerted mechanism or a stepwise mechanism with rate-limiting formation of the phosphorane intermediate (Figure 5). In distinguishing between these models, the same considerations introduced for the Mg^{2+}-catalyzed reaction regarding rate-limiting intermediate formation or breakdown are relevant. Indeed, expulsion of the leaving group from the phosphorane intermediate is even more likely to be rate limiting for the RNase P catalyzed reaction because the 3′-OH of ribose ($pK_a = 12.5-14.8$) (*87*) is a considerably worse leaving group than *p*-nitrophenolate ($pK_a = 7.1$), even assuming the RNase P active site substantially increases its reactivity. Therefore, the best model for RNase P catalysis involves a concerted reaction mechanism.

The small magnitude of the RNase P $^{18}k_{nuc}$ relative to the isotope effect on hydroxide-catalyzed T5PNP hydrolysis (1.068 ± 0.007) indicates a stiffer bonding environment for the nucleophile in the RNase P transition state. This result is inconsistent with free hydroxide acting as the nucleophile in RNase P. In contrast, the RNase P $^{18}k_{nuc}$ is remarkably similar to the value observed for Mg^{2+}-catalyzed T5PNP hydrolysis (1.027 ± 0.013). Therefore, the nucleophiles in these two reactions experience the same stiffness in their respective transition state bonding environments. This result is consistent with Mg^{2+} coordination accounting for activation of the solvent nucleophile in the RNase P active site with a Mg−OH complex ultimately acting as the nucleophile (Figure 5). The isotope effect results cannot formally rule out that a hydrogen bond is responsible for the increased stiffness experienced by the nucleophilic oxygen in the RNase P active site. However, evidence that at least one Mg^{2+} participates in transition state stabilization (*33*) and that a metal ion contacts the R_P nonbridging oxygen atom at the cleavage site (*19*, *20*) also supports the model presented in Figure 1.

CONCLUSIONS

We developed new approaches to determining nucleophile HAIE and applied these approaches to gain new insight into the mechanisms of nonenzymatic and RNA-catalyzed phosphodiester hydrolysis. The nucleophile KIEs presented here for the ADA reaction and Mg^{2+} and RNase P catalyzed phosphodiester hydrolysis provide new insights into the mechanisms of these reactions. The concerted mechanisms indicated by normal $^{18}k_{nuc}$ values for Mg^{2+} catalysis and the RNase P reaction support the notion that this mechanism is most prevalent for intermolecular phosphodiester cleavage, although the specialized environment of an enzyme active site could result in stepwise mechanisms.

The small magnitude of the inverse $^{18}k_{nuc}$ observed for the hydrolytic deamination catalyzed by ADA indicates that cleavage of the carbon−nitrogen bond is not completely rate determining for the enzyme. Additionally, the smaller *intrinsic* isotope effect, compared to hydration of carbon−carbon double bonds, demonstrates a reduction attributable to coordination of the nucleophile by the catalytic Zn^{2+} in the ADA reaction. The similar reduction in $^{18}k_{nuc}$ is observed for metal coordination of the nucleophile in Mg^{2+}-catalyzed phosphodiester hydrolysis, demonstrating that nucleophile isotope effects provide a valuable and general chemical probe for activation of a solvent nucleophile by metal coordination. Application of this isotopic probe to the RNase P catalyzed reaction supports models invoking a metal-coordinated nucleophile. Questions regarding nucleophilic participation in phosphoryl transfer are abundant in many other enzymatic systems. Examples include whether RNase A catalyzes intramolecular phosphoryl transfer in RNA by a concerted or stepwise reaction and whether specific restriction endonucleases utilize metal−hydroxide nucleophiles. The techniques and concepts presented in this current work are applicable to these other systems and hold the potential to provide valuable insight regarding these uncertainties.

ACKNOWLEDGMENT

We are indebted to Dr. Steve Ingalls for generous assistance with development and analysis of the ESI-QMS measurements and Dr. John Morrison (GV Instruments) for the analysis of $^{18}O/^{16}O$ ratios in water and hypoxanthine. We sincerely appreciate Dr. Alvan Hengge's communication of unpublished isotope effect data. We also acknowledge the support and constructive comments on the manuscript by members of the Anderson and Harris laboratories.

REFERENCES

1. Westheimer, F. H. (1987) Why nature chose phosphates, *Science 235*, 1173−1178.
2. Serpersu, E. H., Shortle, D., and Mildvan, A. S. (1986) Kinetic and magnetic resonance studies of effects of genetic substitution of a Ca^{2+}-liganding amino acid in staphylococcal nuclease, *Biochemistry 25*, 68−77.
3. Beebe, J. A., and Fierke, C. A. (1994) A kinetic mechanism for cleavage of precursor tRNA(Asp) catalyzed by the RNA component of *Bacillus subtilis* ribonuclease P, *Biochemistry 33*, 10294−10304.
4. Kirby, A. J., and Younas, M. (1970) The reactivity of phosphate esters. Reactions of diesters with nucleophiles, *J. Chem. Soc. 3*, 1165−1172.
5. Kirby, A. J., and Younas, M. (1970) The reactivity of phosphate esters. Diester hydrolysis, *J. Chem. Soc. 3*, 510−513.
6. Hengge, A. C., Tobin, A. E., and Cleland, W. W. (1995) Studies of transition-state structures in phosphoryl transfer reactions of phosphodiesters of *p*-nitrophenol, *J. Am. Chem. Soc. 214*, 5919−5926.
7. Breslow, R. (1993) Kinetics and mechanism in RNA cleavage, *Proc. Natl. Acad. Sci. U.S.A. 90*, 1208−1211.
8. Gerratana, B., Sowa, G. A., and Cleland, W. W. (2000) Characterization of the transition state structures and mechanisms for the isomerization and cleavage reactions of 3′-*m*-nitrobenzyl phosphate, *J. Am. Chem. Soc. 122*, 12615−12621.
9. Humphry, T., Forconi, M., Williams, N. H., and Hengge, A. C. (2002) An altered mechanism of hydrolysis for a metal-complexed phosphate diester, *J. Am. Chem. Soc. 124*, 14860−14861.
10. Sowa, G. A., Hengge, A. C., and Cleland, W. W. (1997) ^{18}O isotope effects support a concerted mechanism for ribonuclease A, *J. Am. Chem. Soc. 119*, 2319−2320.
11. Hengge, A. C. (2001) Isotope effects in the study of enzymatic phosphoryl transfer reactions, *FEBS Lett. 501*, 99−102.
12. Lahiri, S. D., Zhang, G., Dunaway-Mariano, D., and Allen, K. N. (2003) The pentacovalent phosphorus intermediate of a phosphoryl transfer reaction, *Science 299*, 2067−2071.
13. Beese, L. S., and Steitz, T. A. (1991) Structural basis for the 3′-5′ exonuclease activity of *Escherichia coli* DNA polymerase I: a two metal ion mechanism, *EMBO J. 10*, 25−33.
14. Pingoud, A., and Jeltsch, A. (2001) Structure and function of type II restriction endonucleases, *Nucleic Acids Res. 29*, 3705−3727.
15. Galburt, E. A., and Stoddard, B. L. (2002) Catalytic mechanisms of restriction and homing endonucleases, *Biochemistry 41*, 13851−13860.

16. Piccirilli, J. A., Vyle, J. S., Caruthers, M. H., and Cech, T. R. (1993) Metal ion catalysis in the *Tetrahymena* ribozyme reaction, *Nature 361*, 85−88.
17. Weinstein, L. B., Jones, B. C., Cosstick, R., and Cech, T. R. (1997) A second catalytic metal ion in group I ribozyme, *Nature 388*, 805−808.
18. Sontheimer, E. J., Gordon, P. M., and Piccirilli, J. A. (1999) Metal ion catalysis during group II intron self-splicing: parallels with the spliceosome, *Genes Dev. 13*, 1729−1741.
19. Warnecke, J. M., Furste, J. P., Hardt, W. D., Erdmann, V. A., and Hartmann, R. K. (1996) Ribonuclease P (RNase P) RNA is converted to a Cd(2+)-ribozyme by a single Rp-phosphorothioate modification in the precursor tRNA at the RNase P cleavage site, *Proc. Natl. Acad. Sci. U.S.A. 93*, 8924−8928.
20. Chen, Y., Li, X., and Gegenheimer, P. (1997) Ribonuclease P catalysis requires Mg^{2+} coordinated to the pro-R_P oxygen of the scissile bond, *Biochemistry 36*, 2425−2438.
21. Nobbs, T. J., Williams, S. A., Connolly, B. A., and Halford, S. E. (1998) Phosphorothioate substrates for the SfiI restriction endonuclease, *Biol. Chem. 379*, 599−604.
22. Cleland, W. W. (1995) Isotope effects: determination of enzyme transition state structure, *Methods Enzymol. 249*, 341−373.
23. Schramm, V. L. (1999) Enzymatic transition-state analysis and transition-state analogs, *Methods Enzymol. 308*, 301−355.
24. Northrop, D. B. (2001) Uses of isotope effects in the study of enzymes, *Methods 24*, 117−124.
25. Huskey, W. P. (1991) in *Enzyme Mechanism from Isotope Effects* (Cook, P. F., Ed.) pp 37−72, CRC Press, Boca Raton, FL.
26. Rawlings, J., Cleland, W. W., and Hengge, A. C. (2003) Metal ion catalyzed hydrolysis of ethyl *p*-nitrophenyl phosphate, *J. Inorg. Biochem. 93*, 61−65.
27. Cassano, A. G., Anderson, V. E., and Harris, M. E. (2002) Evidence for direct attack by hydroxide in phosphodiester hydrolysis, *J. Am. Chem. Soc. 124*, 10964−10965.
28. O'Leary, M. H. (1980) Determination of heavy-atom isotope effects on enzyme-catalyzed reactions, *Methods Enzymol. 64*, 83−104.
29. Breslow, R., Chin, J., Hilvert, D., and Trainor, G. (1983) Evidence for the general base mechanism in carboxypeptidase A-catalyzed reactions: partitioning studies on nucleophiles and H2(18)O kinetic isotope effects, *Proc. Natl. Acad. Sci. U.S.A. 80*, 4585−4589.
30. Unrau, P. J., and Bartel, D. P. (2003) An oxocarbenium-ion intermediate of a ribozyme reaction indicated by kinetic isotope effects, *Proc. Natl. Acad. Sci. U.S.A. 100*, 15393−15397.
31. Narlikar, G. J., and Herschlag, D. (1997) Mechanistic aspects of enzymatic catalysis: lessons from comparison of RNA and protein enzymes, *Annu. Rev. Biochem. 66*, 19−59.
32. Smith, D., and Pace, N. R. (1993) Multiple magnesium ions in the ribonuclease P reaction mechanism, *Biochemistry 32*, 5273−5281.
33. Beebe, J. A., Kurz, J. C., and Fierke, C. A. (1996) Magnesium ions are required by *Bacillus subtilis* ribonuclease P RNA for both binding and cleaving precursor tRNAAsp, *Biochemistry 35*, 10493−10505.
34. Kurz, J. C., and Fierke, C. A. (2000) Ribonuclease P: a ribonucleoprotein enzyme, *Curr. Opin. Chem. Biol. 4*, 553−558.
35. Persson, T., Cuzic, S., and Hartmann, R. K. (2003) Catalysis by RNase P RNA: unique features and unprecedented active site plasticity, *J. Biol. Chem. 278*, 43394−43401.
36. Kurz, J. C., and Lee, J. S. (1980) Deuterium and oxygen-18 isotope effects on nucleophilic displacement by monomeric water in aprotic solvants, *J. Am. Chem. Soc. 102*, 5427−5429.
37. Cleland, W. W. (1982) Use of isotope effects to elucidate enzyme mechanisms, *CRC Crit. Rev. Biochem. 13*, 385−428.
38. Werner, R. A., Kornexl, B. E., Rossmann, A., and Schmidt, H. L. (1996) Online determination of $\delta^{18}O$ values of organic substances, *Anal. Chim. Acta 319*, 159−164.
39. Begley, I. S., and Scrimgeour, C. M. (1996) Online reduction of H_2O for δ^2H and $\delta^{18}O$ measurement by continuous-flow isotope ratio mass spectrometry, *Rapid Commun. Mass Spectrom. 10*, 969−973.
40. Goshe, M. B., and Anderson, V. E. (1995) Determination of amino acid isotope ratios by electrospray ionization-mass spectrometry, *Anal. Biochem. 231*, 387−392.
41. Cohn, M., and Urey, H. C. (1938) Oxygen exchange reactions of organic compounds and water, *J. Am. Chem. Soc. 60*, 679−687.
42. Epstein, S., and Mayeda, T. (1953) Variation of oxygen-18 content of waters from natural sources, *Geochim. Cosmochim. Acta 4*, 213−224.
43. Begley, I. S., and Sharp, B. L. (1997) Characterisation and correction of instrumental bias in inductively coupled plasma quadrupole mass spectrometry for accurate measurement of lead isotope ratios, *J. Anal. At. Spectrom. 12*, 395−402.
44. Dahm, S. C., and Uhlenbeck, O. C. (1991) Role of divalent metal ions in the hammerhead RNA cleavage reaction, *Biochemistry 30*, 9464−9469.
45. Jencks, W. P. (1969) Practical Kinetics, in *Catalysis in Chemistry and Enzymology*, Chapter 11, McGraw-Hill, New York.
46. Siew, D., Zahler, N. H., Cassano, A. G., Strobel, S. A., and Harris, M. E. (1999) Identification of adenosine functional groups involved in substrate binding by the ribonuclease P ribozyme, *Biochemistry 38*, 1873−1883.
47. Kline, P. C., and Schramm, V. L. (1993) Purine nucleoside phosphorylase. Catalytic mechanism and transition-state analysis of the arsenolysis reaction, *Biochemistry 32*, 13212−13219.
48. Werner, R. A. (2003) The online $^{18}O/^{16}O$ analysis: development and application, *Isot. Environ. Health Stud. 39*, 85−104.
49. Hendry, P., and Sargeson, A. M. (1989) Metal ion promoted phosphate ester hydrolysis. Intramolecular attack of coordinated hydroxide ion, *J. Am. Chem. Soc. 111*, 2521−2527.
50. Deal, K. A., Hengge, A. C., and Burstyn, J. N. (1996) Characterization of transition states in dichloro(1,4,7-triazacyclononane)-copper(II)-catalyzed activated phosphate diester hydrolysis, *J. Am. Chem. Soc. 118*, 1713−1718.
51. Deck, K. M., Tseng, T. A., and Burstyn, J. N. (2002) Triisopropyltriazacyclononane copper (II): An efficient phosphodiester hydrolysis catalyst and DNA cleavage agent, *Inorg. Chem. 41*, 669−667.
52. Northrop, D. B. (1981) The expression of isotope effects on enzyme-catalyzed reactions, *Annu. Rev. Biochem. 50*, 103−131.
53. Melander, L., and Saunders, W. H. (1980) *Reaction Rates of Isotopic Molecules*, Wiley, New York.
54. Paneth, P., and O'Leary, M. H. (1991) Nitrogen and deuterium isotope effects on the quarternization of N,N-dimethyl-p-toluidine, *J. Am. Chem. Soc. 113*, 1691−1693.
55. Marlier, J. F. (1993) Heavy-atom isotope effects on the alkaline hydrolysis of methyl formate: The role of hydroxide ion in ester hydrolysis, *J. Am. Chem. Soc. 115*, 5953−5956.
56. Westaway, K. C., Fang, Y.-r., Persson, J., and Matsson, O. (1998) Using $^{11}C/^{14}C$ incoming group and secondary α-deuterium KIEs to determine how a change in leaving group alters the structure of the transition state of the S_N2 reactions between meta-chlorobenzyl para-substituted benzenesulfonates and cyanide ion, *J. Am. Chem. Soc. 120*, 3340−3344.
57. Marlier, J. F., Dopke, N. C., Johnstone, K. R., and Wirdzig, T. J. (1999) A heavy-atom isotope effect study of the hydrolysis of formamide, *J. Am. Chem. Soc. 121*, 4356−4363.
58. Hogg, J. L., Rodgers, J., Kovach, I., and Schowen, R. L. (1980) Kinetic isotope-effect probes of transition-state structure. Vibrational analysis of model transition states for carbonyl addition, *J. Am. Chem. Soc. 102*, 79−85.
59. Kurz, L. C., and Frieden, C. (1983) Adenosine deaminase: solvent isotope and pH effects on the binding of transition-state and ground-state analogue inhibitors, *Biochemistry 22*, 382−389.
60. Rishavy, M. A., and Cleland, W. W. (1999) ^{13}C, ^{15}N, and ^{18}O equilibrium isotope effects and fractionation factors, *Can. J. Chem. 77*, 967−977.
61. Weiss, P. M., Cook, P. F., Hermes, J. D., and Cleland, W. W. (1987) Evidence from nitrogen-15 and solvent deuterium isotope effects on the chemical mechanism of adenosine deaminase, *Biochemistry 26*, 7378−7384.
62. Blanchard, J. S., and Cleland, W. W. (1980) Use of isotope effects to deduce the chemical mechanism of fumarase, *Biochemistry 19*, 4506−4513.
63. Bahnson, B. J., and Anderson, V. E. (1989) Isotope effects on the crotonase reaction, *Biochemistry 28*, 4173−4181.
64. Bahnson, B. J., and Anderson, V. E. (1991) Crotonase-catalyzed beta-elimination is concerted: a double isotope effect study, *Biochemistry 30*, 5894−5906.
65. Feder, H. M., and Taube, H. (1952) Ionic hydration: an isotopic fractionation technique, *J. Chem. Phys. 20*, 1335−1336.
66. Wilson, D. K., Rudolph, F. B., and Quiocho, F. A. (1991) Atomic structure of adenosine deaminase complexed with a transition-state analog: understanding catalysis and immunodeficiency mutations, *Science 252*, 1278−1284.

67. Herschlag, D., and Jencks, W. P. (1987) The effect of divalent metal ions on the rate and transition-state structure of phosphoryl-transfer reactions, *J. Am. Chem. Soc. 109*, 4665−4674.
68. Herschlag, D., and Jencks, W. P. (1990) Catalysis of the hydrolysis of phosphorylated pyridines by Mg(OH)+: a possible model for enzymatic phosphoryl transfer, *Biochemistry 29*, 5172−5179.
69. Zhou, D. M., and Taira, K. (1998) The hydrolysis of RNA: From theoretical calculations to the hammerhead ribozyme mediated cleavage of RNA, *Chem. Rev. 98*, 991−1026.
70. Taube, H. (1954) Use of oxygen-isotope effects in the study of hydration of ions, *J. Phys. Chem. 58*, 523−528.
71. Green, M., and Taube, H. (1963) Isotopic fractionation in the OH- -H_2O exchange reaction, *J. Phys. Chem. 67*, 1565−1566.
72. Hunt, H. R., and Taube, H. (1959) The relative acidities of $H_2{}^{18}O$ and $H_2{}^{16}O$ coordinated to a tripositive ion, *J. Phys. Chem. 63*, 124−125.
73. Bagshaw, C. R., Trentham, D. R., Wolcott, R. G., and Boyer, P. D. (1975) Oxygen exchange in the gamma-phosphoryl group of protein-bound ATP during Mg^{2+}-dependent adenosine triphosphatase activity of myosin, *Proc. Natl. Acad. Sci. U.S.A. 72*, 2592−2596.
74. Choate, G. L., Hutton, R. L., and Boyer, P. D. (1979) Occurrence and significance of oxygen exchange reactions catalyzed by mitochondrial adenosine triphosphatase preparations, *J. Biol. Chem. 254*, 286−290.
75. Campbell, F. E., Jr., Cassano, A. G., Anderson, V. E., and Harris, M. E. (2002) Pre-steady-state and stopped-flow fluorescence analysis of *Escherichia coli* ribonuclease III: insights into mechanism and conformational changes associated with binding and catalysis, *J. Mol. Biol. 317*, 21−40.
76. Frank, D. N., and Pace, N. R. (1998) Ribonuclease P: unity and diversity in a tRNA processing ribozyme, *Annu. Rev. Biochem. 67*, 153−180.
77. Shan, S., Kravchuk, A. V., Piccirilli, J. A., and Herschlag, D. (2001) Defining the catalytic metal ion interactions in the *Tetrahymena* ribozyme reaction, *Biochemistry 40*, 5161−5171.
78. Rajagopal, J., Doudna, J. A., and Szostak, J. W. (1989) Stereochemical course of catalysis by the *Tetrahymena* ribozyme, *Science 244*, 692−694.
79. McSwiggen, J. A., and Cech, T. R. (1989) Stereochemistry of RNA cleavage by the *Tetrahymena* ribozyme and evidence that the chemical step is not rate-limiting, *Science 244*, 679−683.
80. Padgett, R. A., Podar, M., Boulanger, S. C., and Perlman, P. S. (1994) The stereochemical course of group II intron self-splicing, *Science 266*, 1685−1688.
81. Yee, D., Armstrong, V. W., and Eckstein, F. (1979) Mechanistic studies on deoxyribonucleic acid dependent ribonucleic acid polymerase from *Escherichia coli* using phosphorothioate analogues. 1. Initiation and pyrophosphate exchange reactions, *Biochemistry 18*, 4116−4120.
82. Gupta, A., DeBrosse, C., and Benkovic, S. J. (1982) Template-prime-dependent turnover of (Sp)-dATP alpha S by T4 DNA polymerase. The stereochemistry of the associated 3′ goes to 5′-exonuclease, *J. Biol. Chem. 257*, 7689−7692.
83. Hengge, A. C., Sowa, G. A., Wu, L., and Zhang, Z. Y. (1995) Nature of the transition state of the protein-tyrosine phosphatase-catalyzed reaction, *Biochemistry 34*, 13982−13987.
84. Usher, D. A., Erenrich, E. S., and Eckstein, F. (1972) Geometry of the first step in the action of ribonuclease-A (in-line geometry-uridine2′,3′-cyclic thiophosphate-^{31}P NMR), *Proc. Natl. Acad. Sci. U.S.A. 69*, 115−118.
85. Bevilacqua, P. C., Brown, T. S., Nakano, S., and Yajima, R. (2004) Catalytic roles for proton transfer and protonation in ribozymes, *Biopolymers 73*, 90−109.
86. Choe, J. Y., Iancu, C. V., Fromm, H. J., and Honzatko, R. B. (2003) Metaphosphate in the active site of fructose-1,6-bisphosphatase, *J. Biol. Chem. 278*, 16015−16020.
87. Herschlag, D., Eckstein, F., and Cech, T. R. (1993) The importance of being ribose at the cleavage site in the *Tetrahymena* ribozyme reaction, *Biochemistry 32*, 8312−8321.

BI049188F